Journal of the Taiwan Institute of Chemical Engineers xxx (xxxx) xxx

Contents lists available at ScienceDirect

Journal of the Taiwan Institute of Chemical Engineers

journal homepage: www.journals.elsevier.com/journal-of-the-taiwan-institute-of-chemical-engineers

Biocompatible neuronal stimulant-embedded poly(γ-benzyl-L-glutamate) peptide-based scaffolds promote differentiation, growth and functional maturation of human induced pluripotent stem cell-derived retinal ganglion cells

Ta-Ching Chen [a,b,c], Yu-Ju Minnie Chou [a,d], Yu-Xuan Wu [e], Jui-En Lo [e], Chia-Yu Lin [f], Yun-Hsiu Tseng [f], Ya-Chun Chu [f], Wei-Li Chen [a,g], Fung-Rong Hu [a,g], Wei-Fang Su [c,f,*], Hung-Chih Kuo [d,**]

[a] Department of Ophthalmology, National Taiwan University Hospital, Taipei 100002, Taiwan
[b] Center of Frontier Medicine, National Taiwan University Hospital, Taipei 10002, Taiwan
[c] Molecular Imaging Center, National Taiwan University, Taipei 10617, Taiwan
[d] Institute of Cellular and Organismic Biology, Academia Sinica, Taipei 11529, Taiwan
[e] Department of Medical Education, National Taiwan University Hospital, Taipei 10002, Taiwan
[f] Department of Materials Science and Engineering, National Taiwan University, Taipei, Taiwan
[g] Department of Ophthalmology, College of Medicine, National Taiwan University, Taipei 100002, Taiwan

ARTICLE INFO

Keywords:
Optic nerve regeneration
Induced pluripotent stem cells
Retinal ganglion cells
Tissue engineering
Polybenzyl glutamate
Glutamic acid

ABSTRACT

Background: To culture human induced pluripotent stem cells(hiPSCs)- derived retinal ganglion cells (RGCs) with appropriate structure and functionality is critical for cell therapy of optic nerve degeneration. In this study, we aimed to assess the effectiveness of three biocompatible scaffolds -poly(γ-benzyl-L-glutamate) (PBG)-based three-dimensional fibrous scaffolds in promoting the structural and functional maturation of hiPSC-derived RGCs.
Methods: The study investigated three scaffolds (1) PBG, (2) PBG with glutamic acid (PBGA20), and (3) PBGA20 with sodium salt (PBGA20-Na). The biocompatibility was evaluated *in vivo* with C57BL/6 mice. Neurite outgrowth was assessed using immunostaining for axon markers, while fluorescence-based Ca2+ imaging and patch-clamp technique were employed to measure neuronal calcium signaling and electrophysiological activity, respectively.
Significant findings: All three PBG-based scaffolds exhibited excellent biocompatibility *in vivo* and effectively supported the directional outgrowth of neurites from hiPSC-derived RGCs while the PBGA20-Na group demonstrated the most favorable outcomes. The presence of glutamic acid in PBGA20 and PBGA20-Na scaffolds led to an increase in calcium signaling within hiPSC-derived RGCs. HiPSC-derived RGCs cultured on PBGA20 and PBGA20-Na scaffolds exhibited an earlier onset of electrophysiological activities with lower thresholds. These promising results provide a foundation for potential sheet transplantation of hiPSC-derived RGCs as cell therapy for optic nerve regeneration.

1. Introduction

Optic neuropathies encompass a range of eye diseases such as glaucoma, optic neuritis, ischemic optic neuropathies, and hereditary optic neuropathies, all of which are characterized by the progressive degeneration of retinal ganglion cells (RGCs) [1]. Failure to treat these conditions can result in permanent blindness [2–4]. RGCs, located in the ganglion cell layer of the inner retina, are responsible for conveying visual information via the optic nerve to the lateral geniculate nucleus and visual cortex in the brain. Restoring vision in cases of optic nerve atrophy is particularly challenging due to the intricate topography and limited regenerative capacity of human neural tissue. As such, it is imperative to develop therapeutic strategies that not only prevent or

* Corresponding author at: Department of Materials Science and Engineering, National Taiwan University, Taipei, Taiwan.
** Corresponding author at: Institute of Cellular and Organismic Biology, Academia Sinica, Taipei 11529, Taiwan.
E-mail addresses: suwf@ntu.edu.tw (W.-F. Su), kuohuch@gate.sinica.edu.tw (H.-C. Kuo).

https://doi.org/10.1016/j.jtice.2023.105257
Received 2 November 2023; Received in revised form 14 November 2023; Accepted 21 November 2023

Abbreviations

hiPSCs	human induced pluripotent stem cells
RGCs	retinal ganglion cells
PBG	poly(γ-benzyl-L-glutamate)
PBGA20	poly(γ-benzyl-L-glutamate)-r-poly(L-glutamic acid)
PBGA20-Na	sodium salt of poly(γ-benzyl-L-glutamate)-r-poly(L-glutamic acid)
PC-12	neuron-like rat pheochromocytoma cells
RDM	retinal differentiation medium
RMM	retinal maturation medium
PLGA	poly(lactic-co-glycolic acid)
PGS/PCL	poly(glycerol sebacate)/polycaprolactone

delay the degeneration of RGCs but also promote their axonal or neuronal regeneration to restore vision [5,6].

In recent years, research on stem cells and progenitor cells of RGCs has shown potential in treating RGC degeneration. Different methods involving stem cells have been studied to reverse or restore RGCs, including stem cell transplantation and replacement, stem cell-mediated neuroprotection, and endogenous transdifferentiation [7]. One approach that has gained attention is the use of RGCs derived from patient-specific human induced pluripotent stem cells (hiPSCs) as a potential cell therapy or as an *ex vivo* disease model [8–10]. Despite encouraging results, two major challenges in the transplantation of hiPSC-derived RGCs are providing structural support for the cells and controlling the orientation and elongation of their axons. Therefore, biomaterials that can guide and promote the outgrowth of RGC neurites in a specific direction could be a valuable tool for cell transplantation.

To achieve the goals of promoting RGC differentiation, maturation, and neurite elongation and orientation, bioengineering techniques have rapidly developed and synthetic polymers of biomaterial have been designed to culture neurons as mimetics of extracellular matrices. Previous studies have proved that hiPSCs cultured with appropriate scaffolds showed enhanced functional maturation [11–14]. Another important concern is whether cultured neurons share similar functions with normal RGCs. To address these challenges, further modification and incorporation of biomolecules or conductive materials to scaffolds are required. To this end, we have developed a serial of synthetic three-dimensional peptide-based bioscaffolds using electrospinning techniques. In previous studies, we demonstrated that a poly(γ-benzyl-L-glutamate) (PBG)-based scaffold facilitated RGC differentiation from hiPSCs and neurite outgrowth. Building upon this success, we further designed two PBG-based scaffolds containing a neuronal stimulant (i.e., glutamic acid): (1) poly(γ-benzyl-L-glutamate)-r-poly(L-glutamic acid) (PBGA20) and (2) the sodium salt of PBGA20 (PBGA20-Na), the latter of which has additional ionic conductivity [15,16]. Our findings showed that directional and extended neurite outgrowth from neuron-like rat pheochromocytoma (PC-12) cells cultured on the PBGA20-Na scaffold was twice as long as that from cells grown on a conventional biopolymer, polycaprolactone (PCL) [15].

Based on our previous work, we were motivated to investigate whether modified scaffolds with aligned fibers could enhance the directional outgrowth of neurites from iPSC-derived RGCs compared to unaligned substrates. Additionally, we were interested in exploring whether neuronal stimulant-embedded scaffolds, such as PBGA20 and PBGA20-Na, could further promote the differentiation and maturation of hiPSC-derived RGCs for potential clinical applications. In this study, we conducted morphological, molecular, and physiological analyses to comprehensively evaluate the directed differentiation, maturation, and growth of hiPSC-derived RGCs cells on the aforementioned PBG-based scaffolds. Firstly, we evaluated and compared the scaffolds' abilities to promote RGC differentiation from hiPSCs and guide the orientation of neurite growth. Secondly, we examined whether the addition of glutamic acid, an excitatory neurotransmitter, to the peptide-based scaffold contributes to the neuronal activity of hiPSC-derived RGCs. Finally, we recorded the electrophysiological activity of the RGCs to explore whether the scaffolds' electroactive properties could promote neuronal cell maturation without additional conductive materials and electrical stimulation. Our results suggested PBGA20-Na scaffold as the best scaffold to promote the differentiation, neurite outgrowth, and the electrophysiological activity of hiPSC-derived RGCs. This study will be the first to investigate the functional neuronal activities and determine the lineage of hiPSC-derived RGCs cultured on PBG-based biocompatible scaffolds.

2. Materials and methods

2.1. Culture and differentiation of hiPSC-derived RGCs

The hiPSCs were cultured according to a previously described protocol [16]. Briefly, hiPSCs were maintained on mouse embryonic fibroblasts as a feeder layer in culture plates containing DMEM/F12 (Gibco) supplemented with 20% knockout serum replacement (Gibco), 1% non-essential amino acids (Gibco), 0.5% L-glutamine (Gibco), and 10 ng/mL basic fibroblast growth factor (234-FSE-025/CF, R&D Systems). The culture plates were kept in a 37℃ incubator under 5% CO2, and the medium was replaced daily. The differentiation of hiPSCs into RGC-like cells was induced using a previously published protocol [12]. Initially, hiPSCs were dissociated into single cells using Accutase (eBioscience) and allowed to re-aggregate (at 9000 cells/well) in V-bottomed 96-well plates (Costar) containing retinal differentiation medium (RDM: Gibco's Minimal Essential Medium supplemented with 20% knockout serum replacement, 0.1 mM non-essential amino acids, 1 mM pyruvate, 0.1 mM 2-mercaptoethanol, 100 U/mL penicillin, 100 μg/mL streptomycin, 20 μM Y-27632 (Merck Millipore), and 3 μM IWR-1e (Merck Millipore)). Matrigel (BD Bioscience) was added to the cells for 10 days (from Day (D) 2 to D12). On D12, the cell aggregates were transferred to 24-well plates (Costar) containing RDM with 0.5% Matrigel and 1% FBS (Merck Millipore). From D15 to D18, 3 μM CHIR99021 (Merck Millipore) and 100 nM SAG (Merck Millipore) were added to the cultures. On D18, the medium was replaced with FBS-free retinal maturation medium (RMM: DMEM/F12 supplemented with N-2-containing GlutaMAX Supplement (Gibico), 100 U/mL penicillin, and 100 μg/mL streptomycin). On D24 (3 days prior to the adherent culture), 10% FBS and 0.5 μM retinoic acid (R26265, Sigma) were added to the RMM. On D27, the cell aggregates were transferred to either 3% Matrigel-coated scaffolds or cover glasses in 24-well plates (Costar) for adherent culture in RMM containing 10% FBS and 100 ng/mL brain-derived neurotrophic factor (BDNF; 248-BD, R&D Systems). During the differentiation process, we initially used immunofluorescence staining to identify hiPSC-derived RGC cells, employing RGC-specific antibodies against MATH5 and BRN3B on adherent culture. On average, 70% of the hiPSC-derived RGC cells expressed these markers. For measuring the concentration of glutamate and cytokines on glass or PBG-based scaffolds, we selected hiPSC-derived RGCs expressing the RGC surface antigen THY1, also known as CD90 (CBL415, Sigma), using flow cytometry to ensure the purity of hiPSC-derived RGCs.

2.2. Electrospun PBG-based scaffolds with aligned fibers

The PBG used in this study was prepared following previously described methods [15,16]. To prepare PBGA20, 2.5 g of PBG powder was dissolved in 62.5 mL of dichloroacetic acid, then 1.9 mL of hydrogen bromide (33 wt% in acetic acid) was added, and the mixture was stirred at 31°C for 15 min. The resulting solution was precipitated in ether, washed with ether and methanol, and vacuum dried overnight at 40°C to yield PBGA20 (containing 20 mol% poly(α-L-glutamic acid) and 80 mol % PBG). For the fabrication of scaffolds with aligned fibers, PBG and

PBGA20 were separately dissolved in a co-solvent of tetrahydrofuran and N,N-dimethylacetamide at co-solvent ratios of 8:2 (v/v) and 9:1 (v/v) for PBG and PBGA20, respectively, overnight. The electrospun fibrous scaffolds were collected on either cover glasses or indium tin oxide glasses. To prepare the PBGA20-Na scaffold, the PBGA20 scaffold was immersed in a 0.2 M NaOH solution at room temperature for 30 min, rinsed with distilled water to remove any residual NaOH, and vacuum dried at 40–50°C overnight.

2.3. Scanning electron microscopy

The adherent cells and fibrous structure of the scaffolds were observed using scanning electron microscopy (SEM) (SM-6700F, JEOL). The specimens were washed with phosphate-buffered saline (PBS) and then fixed with 2.5% glutaraldehyde in 0.1 M cacodylate buffer (pH 7.4) for 1 hour at room temperature. The samples were then post-fixed with 1% osmium tetroxide in 0.1 M cacodylate buffer (pH 7.4) for 1 hour, followed by dehydration through a graded ethanol series and dried using a critical point dryer. The specimens were then coated with a thin layer of gold-palladium and ready for SEM observation.

2.4. Real-time polymerase chain reaction

RNA was extracted from the cells using the TRIzol reagent (Invitrogen) according to the manufacturer's instructions. Following extraction, the RNA extract was treated with DNaseI (DNA-free kit; Ambion) to remove any genomic DNA contamination. Next, cDNA was synthesized using SuperScript III (Invitrogen) with oligo(dT) and random hexamers. Real-time polymerase chain reaction (qPCR) was carried out using a 7500 Fast Real-Time PCR system (Applied Biosystems). The qPCR protocol included an initial hold at 42°C for 5 min, followed by an incubation at 95°C for 10 s, and then 40 cycles of 95°C for 5 s and 60°C for 31 s. All primers used in this study are listed in Supplementary Table 1. The mRNA expression levels of the target genes were determined from the threshold cycle values obtained from the qPCR assay (Table 1).

2.5. Immunofluorescence staining

The cells were fixed with 4% paraformaldehyde for 15 min at ambient temperature. After washing twice with PBS, the cells were permeabilized with 0.1% Triton X-100 (Merck Millipore) for 15 min and then blocked with 2% bovine serum albumin (Sigma) for 60 min at ambient temperature. Thereafter, the samples were incubated overnight at 4℃ with the following primary antibodies (diluted 1:100 in blocking solution): mouse anti-brain-specific homeobox/POU domain protein 3B (BRN3B; sc-514474, Santa Cruz), mouse anti-ISLET1 (ab109517, Abcam), mouse anti-MATH5 (ab229245, Abcam), mouse anti-GluN1 (MAB363, Merck Millipore), and rabbit anti-beta tubulin III (TUJ1; 2146S, Cell Signaling). After washing three times with PBS, the samples were incubated with the corresponding species-specific Alexa Fluor 488- or Alexa Fluor 568-conjugated secondary antibodies (1:1000 dilution) for 60 min at ambient temperature in the dark. The cells were then washed again three times with PBS and mounted in an anti-fade mounting medium containing 4′,6-diamidino-2-phenylindole (DAPI; 40043, Biotium) before examination under a fluorescence microscope.

2.6. Cytokine array

In total, 1 mL of culture medium was collected from each experimental group on days 40, 44, and 48 of adherent culture and subjected to overnight vacuum freeze-drying using the VirTis Benchtop K Freeze Dryer (SP Industries Inc.). The resulting pellets were then resuspended in 1 mL of basal medium, and the cytokines secreted by the cells were detected using the Human Neuro Antibody Array I (ab211062, Abcam) according to the manufacturer's instructions. The levels of cytokines in each sample were determined in duplicate and normalized to those of the positive control spots. The data for each group were analyzed in triplicate.

2.7. In vivo experiments with the biodegradable scaffolds

All animal experiments were conducted in accordance with the animal guidelines of the institution and approved by the Institutional Animal Care and Use Committee of the Laboratory Animal Center, National Taiwan University College of Medicine (IACUC approval number: 20180467). Male C57BL/6 mice were obtained from the National Laboratory Animal Center, Taipei, Taiwan. Prior to surgery, the mice were anesthetized by intraperitoneal injection of 50 mg/kg ketamine and 10 mg/kg xylazine. A sterile 30G × 1/2 inch needle was used to puncture a hole posterior to the corneal limbus. After the initial puncture, a 1 mm2 piece of scaffold was carefully inserted into the vitreous through the use of a blunt 30G needle. The contralateral eye of each mouse was used as a control, and only the initial puncture was performed. After the surgery, the mice were placed in a warm chamber for recovery.

2.8. Histological examination

After a 2-week post-surgery period, the mice were humanely euthanized using CO2 inhalation followed by cervical dislocation. The eyeballs were carefully removed and fixed in 4% paraformaldehyde at room temperature overnight. Subsequently, the samples were embedded in paraffin wax, sectioned into thin slices, and stained with hematoxylin and eosin. The tissue sections were examined under a light microscope to evaluate the degree of inflammatory response.

2.9. Fura-2 AM calcium imaging

Fura-2-acetoxymethyl ester (Fura-2 AM) calcium imaging of the hiPSC-derived RGCs was conducted in an extracellular solution (13 mM glucose, 5 mM KCl, 1 mM $MgCl_2$, 145 mM NaCl, 2 mM $CaCl_2$, and 10 mM HEPES). The cells were first washed twice in the extracellular solution and then incubated with 2.5 μM Fura-2 AM reagent(ab120873, Abcam) for 30 min at 37°C in the dark. Then, after removal of the Fura-2 AM reagent, the Fura-2 fluorescence emission at 510 nm was recorded every 60 s following excitation at 340 and 380 nm. The relative change in intracellular Ca^{2+} (ΔCa^{2+}), calculated as the ratio of the Fura-2 fluorescence intensities following excitation at 340 and 380 nm (F340/F380), was determined and normalized to the mean basal fluorescence reading according to the following formula: $\Delta Ca^{2+} = \Delta F/F = (F - F_{rest})/$

Table 1
. Primer sequences used for the quantitative real-time PCR analysis of hiPSC-derived retinal progenitors and RGCs.

Gene	Forward	Reverse
Rx	CCGTCCCTAAGCGTGCTTTC	ACTGGGAGCTTCACTAATTTGCTCA
Pax6	TTTAAAGATCCTGGAGGTGGACATA	GCTCAGGTGCTCGGGTTCTA
Chx10	AACCCAATCTGGCTGGTAAATGA	CAGCAGGCCCTTAATGCGTA
Brn3B	TGACACATGAGCGCTCTCACTTAC	ACCAAGTGGCAAATGCACCTA
Math5	CCCTAAATTTGGGCAAGTGAAGA	CAAAGCAACTCACGTGCAATC
Tuj1	GGCCAAGGGTCACTACACG	GCAGTCGCAGTTTTCACACTC

Primer sequences used for the qPCR analysis

F_{rest}, where F is the F340/F380 ratio at any given time and F_{rest} is the mean fluorescence of the given well prior to the addition of the nucleotide ATP (for evoking the Ca^{2+} response). Hoechst solution (#33342, Bio-Rad) was used for the specific staining of the nuclei of live cells.

2.10. Measurement of glutamate secretion into the culture medium

To assess the secretion of glutamate into the culture medium, hiPSC-derived RGCs were plated at a density of 10,000 cells/cm2 and grown in glutamate-free RMM at 37°C with 5% CO2. After 24 hours, the culture medium was collected and stored at -20°C. We performed a cell count after removing the media to normalize our results for glutamate or cytokine concentration. Glutamate levels were measured by transferring 1 mL of the thawed sample to the wells of white luminescent 96-well plates and assaying it using the Glutamine/Glutamate-Glo™ Assay Kit (#J8021, Promega) according to the manufacturer's instructions. Luminescence was measured using a luminometer (EnSpire Multilabel Plate Reader, Perkin-Elmer).

2.11. Viruses

The National RNAi Core Facility at Academia Sinica in Taiwan provided all viruses used in the study, while the plasmid pAAV-EF1a-GCaMP6s-WPRE-pGHpA was purchased from Addgene (Plasmid #67526). hiPSC-derived RGCs were infected with the pAAV-Brn3b-GCaMP6s-WPRE-pGHpA vector for the calcium activity experiments.

2.12. GCaMP6s analysis

Two days after infection with pAAV-Brn3b-GCaMP6s-WPRE-pGHpA, hiPSC-derived RGCs were transferred to a 15μ-Slide 2 Well slide (80286, ibidi) along with the scaffolds and cover glasses. Cells were imaged using a confocal microscope (Leica SP8) with a 10× objective at 37°C and 5% CO2. ImageJ software was used to process the GCaMP6s imaging data. For the glutamate experiment, stimulation-triggered responses before and after the addition of 50 μM D-2-amino-5-phosphonopentanoic acid (AP-5; A8054, Sigma) were recorded. The recording was performed 30 minutes after drug administration, and the maximum ΔF/F amplitude within a 5-second window was calculated.

2.13. Electrophysiological activity recording and neurite length analysis of hiPSC-derived RGCs

To investigate whether hiPSC-derived RGCs function as mature neurons, patch-clamp detection was used to record their electrophysiological activity. Whole-cell recordings were obtained using an electrode pipette filled with intracellular solution (131 mM K-gluconate, 20 mM KCl, 8 mM NaCl, 2 mM EGTA, 10 mM HEPES, 2 mM MgATP, and 0.3 mM MgGTP), and the bathing solution (pH 7.2) contained 2.5 mM KCl, 119 mM NaCl, 26.2 mM NaHCO3, 2.5 mM KCl, 1 mM NaH2PO4, 1.3 mM MgSO4, and 11 mM glucose. The access resistance of the electrode pipettes ranged between 4 and 6 MΩ. The resting membrane potential was approximately 0 pA. After a 5-minute stabilization period in current-clamp mode, ramp current injection was initiated to measure action potential activity. Spontaneously beating RGCs were recorded via whole-cell current clamping. The recording of excitatory postsynaptic currents (EPSCs) suggested that the differentiated RGCs were receiving functional synaptic inputs. The whole-cell patch-clamp recordings were obtained at 25°C using an Axonpatch 200B amplifier (Molecular Devices), filtered at 5 kHz, and sampled at 10 kHz with a Digidata 1440A interface (Molecular Devices) controlled by pCLAMP version 10.4 (Molecular Devices).

To analyze neurite length and orientation of the hiPSC-derived RGCs, ImageJ software was used. Neurite lengths were measured from the cell body to the end of the neurite, and neurite orientation was measured as the angle of the neurites. Three repeat measurements were performed for each experimental group, and more than 85 neurites were measured in each sample.

2.14. Statistical analysis

Statistical analysis was performed using GraphPad Prism software. Student's t-test or analysis of variance was used where appropriate, and the Kruskal–Wallis H test (a non-parametric statistical test) was used to evaluate the statistical difference in data between the various experimental groups because neurite lengths did not follow a normal distribution. Group differences with a p value of less than 0.05 were considered statistically significant.

3. Results

3.1. Aligned PBG-based scaffolds promote the RGC differentiation from human iPSCs

To generate RGCs, hiPSCs were subjected to previously described methods with minor modifications for in vitro RGC differentiation [16], we oberserved the morphology of hiPSC-derived RGCs after 3 and 7 days with adhenrent culture Fig. 1 (a). First, the culture of hiPSC-derived RGCs onto alinged poly(γ-benzyl-L-glutamate)-based scaffolds (PBG, PBGA20, and PBGA20-Na) revealed that the hiPSC-derived RGCs were allowed to adhere to the three scaffolds or cover glass (control group), and their appearance was examined using bright-field microscopy and scanning electron microscope (SEM) image after 3 days of adherent culture Fig. 1 (b, c and d). Immunofluorescence staining analysis with antibodies against neuronal antigen (TUJI) and RGC-associated antigens (BRN3B and MATH5) revealed that putative RGC populations expressing both neuronal and RGC-associated biomarkers could be readily detected in the hiPSC-derived RGCs grown onto the PBG scaffolds, suggesting the PBG scaffolds were able to support RGC differentiation from hiPSCs in vitro Fig. 1 (e and f). Furthermore, quantitative PCR analysis showed that the expression of retinal progenitor-related genes, such as Rx, Pax6 and Chx10 genes, was downregulated in the cell population cultured on all three PBG-based scaffolds during the in vitro differentiation from D3 to D7. Of note, Rx gene expression was significantly downregulated in all scaffold groups relative to the level in the control group. The levels of Pax6 expression in the PBG and PBGA20-Na scaffold groups were also significantly lower than that in the control group. We also examined the mRNA expression levels of Math5, Brn3 and Tuj1, which are typically genes expressed in RGCs. The mRNA levels of Math5 and Brn3b tended to be higher on D7 than on D3 in all experimental groups. However, the upregulation of Math5 relative to the control group level was significantly higher in the PBGA20-Na group only on D7 Fig. 1 (g). Together, these findings collectively suggest that all PBG-based scaffolds promote the differentiation of hiPSC-derived RGCs, and the PBGA20-Na group might exhibit the highest efficacy.

3.2. PBGA20-Na scaffold promotes the longest neurite outgrowth of hiPSC-derived RGCs

We further investigated the effects of the three fibrous scaffolds on neurite outgrowth by immunostaining for the BRN3B and TUJ1 proteins. Abundantly aligned TUJ1 proteins, indicating extended neurites navigating notable distances, were observed in hiPSC-derived RGCs cultured on the PBG-based scaffolds on D3 and D7. By contrast, the control group exhibited only limited neurite outgrowth distance on D7 Fig. 2 (a). The distribution of neurite lengths on the adherent cultures on D3 and D7 revealed that the neurites of hiPSC-derived RGCs cultured on the PBG-based scaffolds had already elongated on D3 and further extended on D7 Fig. 2 (b). The average neurite length was significantly longer for hiPSC-derived RGCs cultured on the PBG-based scaffolds compared to those on the cover glass, with the neurites of the PBGA20-Na group notably being he longest on both D3 and D7 Fig. 2 (c). The

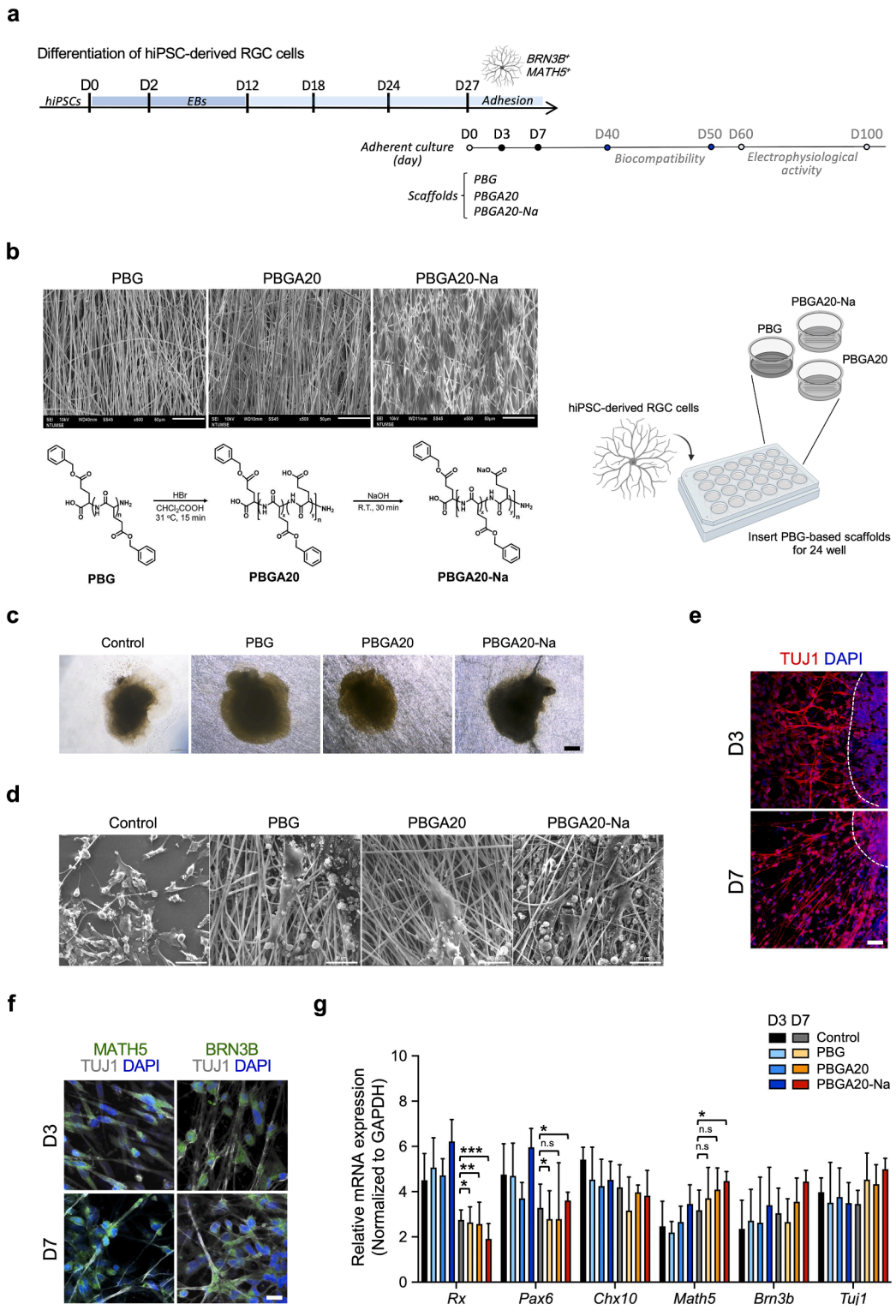

Fig. 1. Induction of hiPSC differentiation into RGC-like cells on PBG, PBGA20, and PBGA20-Na scaffolds.
a. The schematic diagram of the whole process of this study. **b.** The fabrication and chemical formulas of aligned-PBG, PBGA20, and PBGA20-Na (left). The schematic diagram of the culture plate for culturing hiPSC-derived RGCs onto PBG-based scaffolds (right). **c.** Bright-field microscopy images of the hiPSC-derived RGCs cultured on a cover glass (control) and the PBG-based scaffolds on D3 of adherent culture. Scale bar: 20 μm. **d.** Scanning electron microscope images of hiPSC-derived RGCs cultured on a cover glass (control) and the PBG-based scaffolds on D3 of adherent culture. Scale bar: 20 μm. **e.** Immunofluorescence staining of hiPSC-derived RGCs cultured on the PBG-based scaffolds with neuron-specific antibodies against β-tubulin (TUJ1) and DAPI stain on D3 and D7 of adherent culture. Scale bar: 100 μm. **f.** Immunofluorescence staining of hiPSC-derived RGCs cultured on the PBG-based scaffolds with RGC-specific antibodies against MATH5, BRN3B, and DAPI stain on D3 and D7 of adherent culture. Scale bar: 2 μm. **g.** RT-qPCR analysis of the mRNA expression levels of retinal progenitor-related genes: *Rx, Pax6* and *Chx10*, and RGC-related gene: *Math5* and *Brn3b*, and *Tuj1* used as a neuronal-associated gene in hiPSC-derived RGCs cultured on the PBG-based scaffolds on D3 and D7 of adherent culture. Data are shown as the mean ± SEM, n = 3–6. P-values were determined by Student's t-test (two-tailed test) in G, $*p < 0.05$, $**p < 0.01$, $***p < 0.001$, n.s., not significant. All the schematic diagrams were drawn using the BioRender.com.

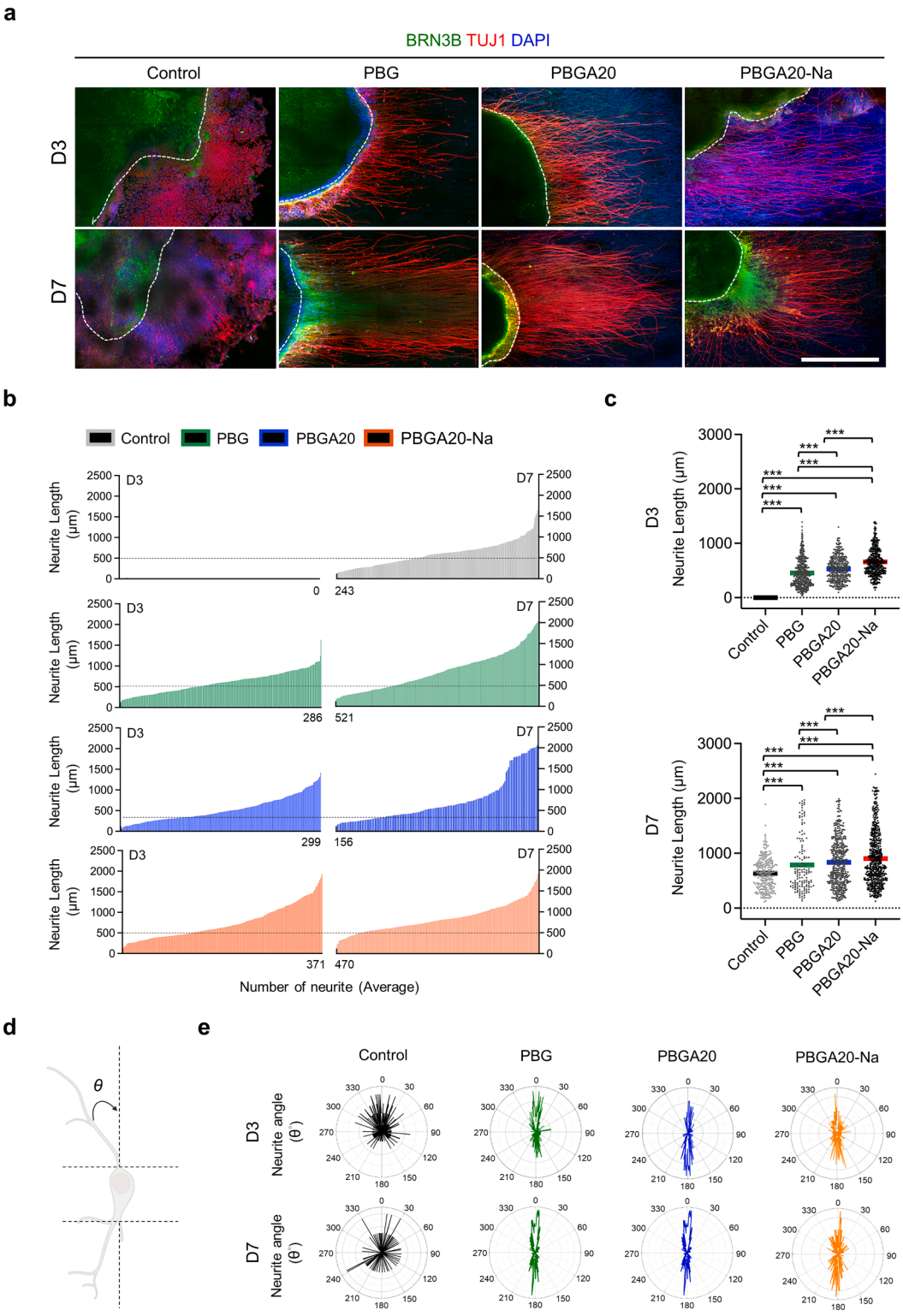

Fig. 2. Neurite outgrowth and orientation of hiPSC-derived RGCs cultured on the PBG-based scaffolds.
a. Representative immunofluorescence images of hiPSC-derived RGCs cultured on a cover glass (control) or PBG-based scaffolds on D3 and D7 of adherent culture. hiPSC-derived RGCs were stained with RGC-specific antibodies against BRN3B, neuron-specific antibodies against β-tubulin (TUJ1) and DAPI stain. Scale bar: 250 μm. b. The probability distribution of the neurite lengths of hiPSC-derived RGCs cultured on a cover glass (control) or the PBG-based scaffolds on D3 and D7 of adherent culture. c. The average neurite lengths of hiPSC-derived RGCs cultured on a cover glass (control) or the PBG-based scaffolds on D3 and D7 of adherent culture were analyzed by ImageJ. d. Schematic illustration of the measurement of the angles of a neurite. e. Orientation of neurites from hiPSC-derived RGCs cultured on a cover glass (control) or the PBG-based scaffolds on D3 and D7 of adherent culture, revealed that the aligned fibers of the scaffolds could guide the growth of neurites. Data are shown as mean ± SEM, n = 3–6. P-values were determined by two-way ANOVA with Tukey's post hoc test in c, $***p < 0.001$. The schematic diagram in d was drawn using the BioRender.com.

angles of the neurites, which represent the overall orientation of neurite outgrowth, were also measured. Our results revealed that the aligned fibers of the scaffolds could guide the growth of these neuronal processes. Moreover, a larger distribution of neurite angles within 0–30° suggested that hiPSC-derived RGCs cultured on the PBG-based scaffolds tended to run in the same direction compared to those cultured on the cover glass Fig. 2 (d and e). These results confirmed the feasibility of using aligned PBG-based scaffolds to promote the extension and orientation of neurites of hiPSC-derived RGCs, with the PBGA20-Na scaffold being the best among the three scaffolds.

3.3. Glutamate release promotes optimal neuronal activity in hiPSC-derived RGCs cultured on the PBGA20-Na scaffold

Since glutamate is an excitatory neurotransmitter that promotes synaptic transmission and neurogenesis in RGCs, all PBG-based scaffolds were designed to contain glutamic acid as a stimulant. We first detected the concentration of glutamate in cell-free culture media, which showed no significant differences in glutamate levels between the cover glass and PBG-based scaffolds on D3 and D7. Next, we tested whether PBG-based scaffolds could promote glutamate release from hiPSC-derived RGCs. All hiPSC-derived RGCs cultured on the PBG-based scaffold groups showed significantly higher levels of glutamate in the culture

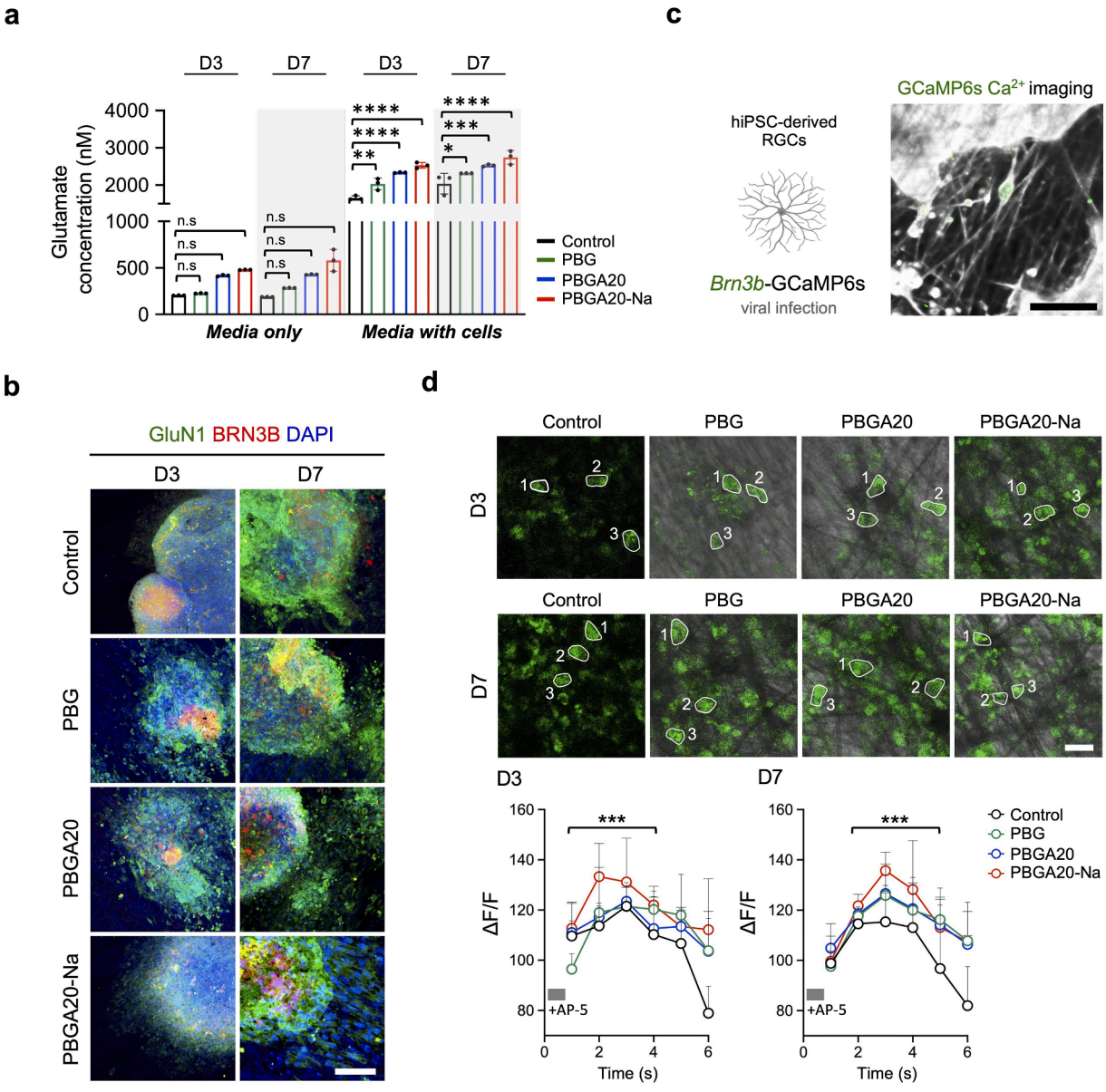

Fig. 3. Detecting glutamate release and calcium imaging of hiPSC-derived RGCs cultured on the PBG-based scaffolds.
a. The concentrations of glutamate in media were assessed with Glutamine/Glutamate-Glo™ Assay Kit from the cover glass (control) and PBG-based scaffolds with and without cultured hiPSC-derived RGCs, on day D3 and D7. b. Immunofluorescence staining of hiPSC-derived RGCs cultured on a cover glass (control) or PBG-based scaffolds on day D3 and D7 of adherent culture. hiPSC-derived RGCs were stained with RGC-specific antibodies against BRN3B, NMDA receptor-specific antibodies against GluN1, and DAPI stain. Scale bar: 50 μm. c. Representative confocal microscopy image of hiPSC-derived RGCs bearing pAAV-Brn3b-GCamp6s. Scale bar: 10 μm. d. The time-series changes in fluorescence intensity ΔF/F of hiPSC-derived RGCs expressing pAAV-Brn3b-GCamp6s cultured on a cover glass (control) or the PBG-based scaffolds on D3 and D7, are depicted with the absence and presence of AP-5, an NMDA antagonist. Scale bar: 2 μm. Quantification of fluorescence data is graphed below, comparing PBGA20-Na to the control. Data are shown as the mean ± SEM, n= 3. P-values were determined by Student's t-test (two-tailed test) in a and d, $*p < 0.05$, $**p < 0.01$, $***p < 0.001$, n.s., not significant.

media compared to those cultured on the cover glass Fig. 3 (a). We subsequently examined the expression of NMDA receptors, which are receptors for glutamate, and we found that GluN1 protein, a subunit of the NMDA receptors, were expressed in hiPSC-derived RGCs cultured in all groups, as observed through immunostaining for the BRN3B and GluN1 proteins Fig. 3 (b). The expression of GluN1 was statistically higher in D7 compared to D3 in every group, respecively. (Fig S3) To investigate whether different concentrations of glutamate within the PBG-based scaffolds cause varying levels of neuronal activity, we conducted the Fura-2 AM assay to detect the presence of intracellular calcium before and after the addition of ATP as an indicator of neuronal activity. The F340/F380 ratio was also calculated to quantify the intracellular calcium level. We found that the PBGA20 and PBGA20-Na groups had significantly higher calcium signals than the other groups on D3 Fig. S1 (a and b). To further confirm the calcium signal from hiPSC-derived RGCs, we constructed the viral vector pAAV-Brn3b-GCaMP6s, which contained the Brn3b promoter, enabling us to specifically track the dynamic calcium changes of hiPSC-derived RGCs. The hiPSC-derived RGCs were first infected with the viral vector and then cultured on the three PBG-based scaffolds or cover glass. Real-time imaging was performed and recorded on D3 and D7 Fig. 3 (c). The intensity of Ca2+ signals decreased gradually a short period after the addition of selective NMDA receptor antagonist (AP-5), which inhibits the receptor activity by competitively binding to its glutamate-binding site. The measurement of Ca2+ signals showed that hiPSC-derived RGCs cultured on the PBG-based scaffolds exhibited significantly higher levels of Ca2+ fluxes (ΔF/F) on D7 compared to those in the control group. Additionally, the hiPSC-derived RGCs cultured on the PBGA20-Na exhibited a significantly higher influx of Ca2+ (ΔF/F) on D3 and D7 than those other groups Fig. 3 (d). Similar findings were obtained in the Ca2+ imaging from the Fura-2 AM assay. Collectively, based on the results of Fura-2 AM and Brn3b-GCaMP6 assays, we assume that the difference in Ca2+

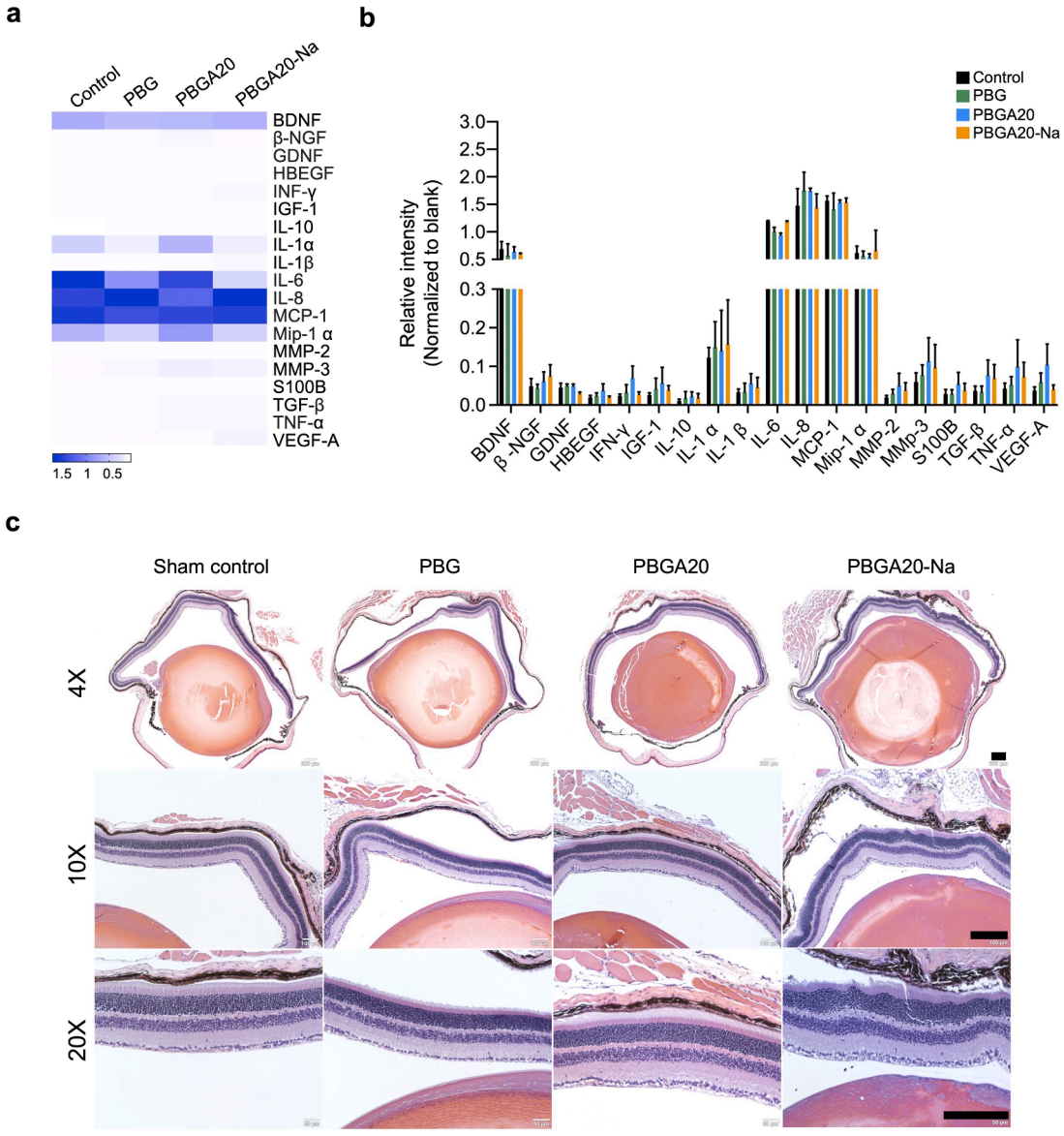

Fig. 4. Biocompatibility of PBG-based scaffolds and immune response of hiPSC-derived RGCs are investigated *in vitro* and *in vivo*.
a. Heatmap of immune response-associated growth factors, chemokines and cytokine protein levels in the culture media of hiPSC-derived RGCs cultured on a cover glass (control) or the PBG-based scaffolds was examined for 40-50 days using a human cytokine antibody array. b. Quantitative analysis of the immune response-associated growth factors and cytokine secreted from hiPSC-derived RGCs cultured on a cover glass (control) or the PBG-based scaffolds. c. Hematoxylin and eosin staining of the retinas of mice after sham treatment or the PBG-based scaffolds implantation for 2 weeks. No immune-responsive characteristics were observed in the groups transplanted with PBG-based scaffolds. Scale bars: 200 μm. Data are shown as mean ± SEM, n = 3–6.

influx between the hiPSC-derived RGCs cultured on the PBG-based scaffolds and those on the cover glass is due to the different levels of glutamate, particularly evident on D7. Moreover, PBGA20-Na exhibited the highest neuronal activity, accompanied by the highest glutamate release from hiPSC-derived RGCs compared to the other groups.

3.4. PBG-based scaffolds demonstrate no detectable inflammatory effects in cultured hiPSC-derived RGCs and exhibit good biocompatibility of the scaffolds

The PBG-based scaffolds were designed to assist in RGC tissue engineering by promoting the outgrowth of RGCs. However, a concern is

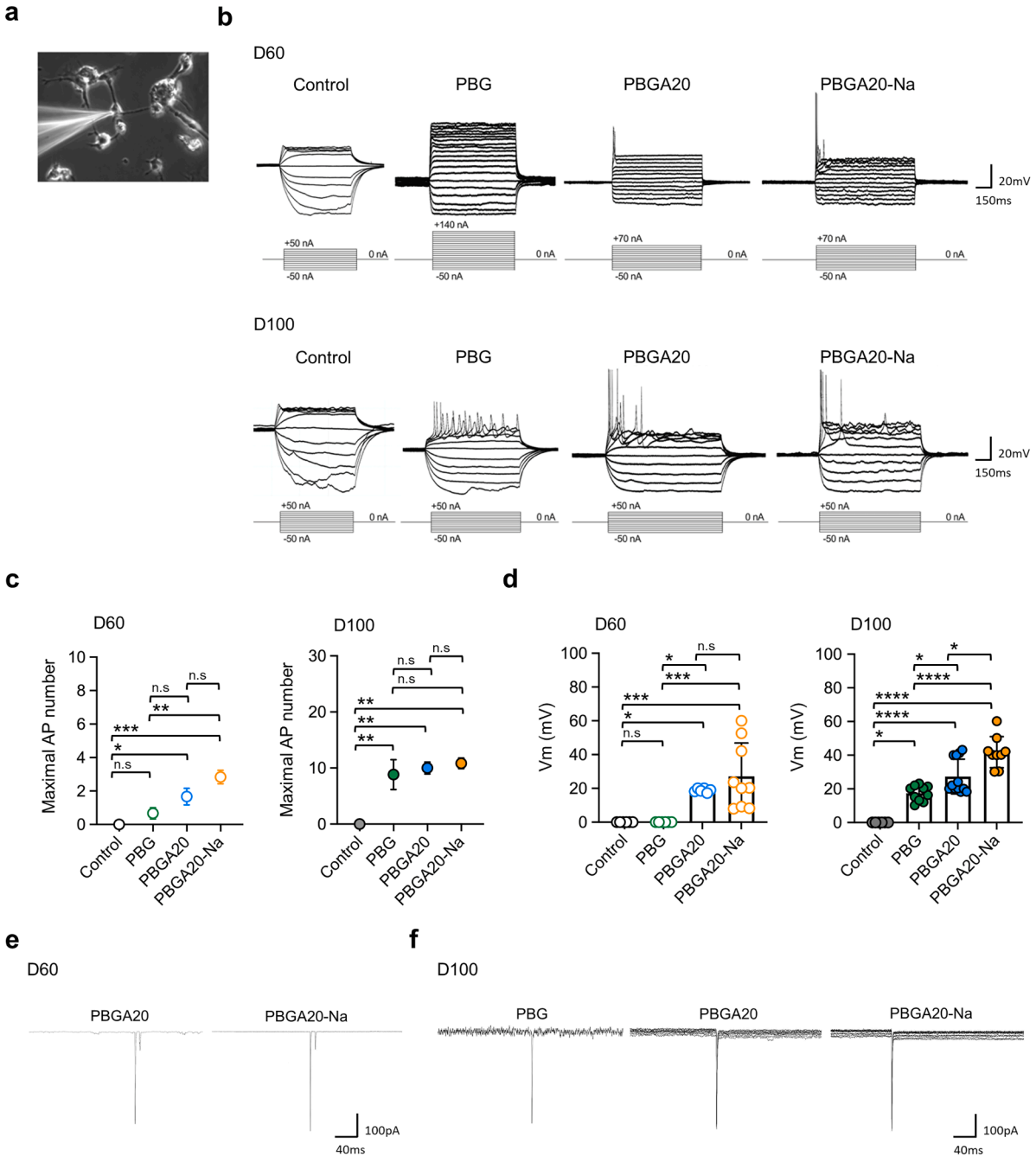

Fig. 5. The functional electrophysiological properties of hiPSC-derived RGCs cultured on the PBG-based scaffolds.
a. Representative image of the patch-clamp recording of hiPSC-derived RGCs cultured on a cover glass (control) or the PBG-based scaffolds. b. Voltage responses of hiPSC-derived RGCs were determined by whole-cell current-clamp recordings in response to a graded series of intracellular current pulses while cultured on either a cover glass (control) or the PBG-based scaffolds, on D60 and D100. c. Number of hiPSC-derived RGCs that fired APs when cultured on a cover glass (control) or the PBG-based scaffolds on D60 and D100. d. Quantification of spike amplitudes of hiPSC-derived RGCs during applied current series of 70 or 50 nA cultured on a cover glass (control) or the PBG-based scaffolds, on D60 and D100.
e-f. Evoked excitatory postsynaptic currents (EPSCs) of hiPSC-derived RGCs cultured on a cover glass (control) or the PBG-based scaffolds on D60 and D100, following stimulation by a single current pulse. EPSCs were readily detected in cells on the PBGA20 and PBGA20-Na scaffolds on D60 (E) and were also recorded in cells on all three scaffolds on D100 (F). Data are shown as the mean ± SEM, n = 3–9. P-values were determined by two-way ANOVA with Tukey's post hoc test in c and d, $*p < 0.05$, $**p < 0.01$, $***p < 0.001$, $****p < 0.0001$, n.s., not significant.

that the synthetic scaffolds may cause local inflammatory responses due to their degradation. To elucidate whether the PBG-based scaffold material influences the release of immune response-associated growth factors, chemokines, or cytokines from cultured hiPSC-derived RGCs, we investigated whether hiPSC-derived RGCs cultured on a cover glass had any advantages over those grown on the PBG-based scaffolds in terms of their immune response. Then, hiPSC-derived RGCs cultured on the PBG-based scaffolds for 40–50 days of adherent culture were examined using a human cytokine antibody array Fig. 4 (a). The protein levels of the growth factors: brain-derived neurotrophic factor (BDNF), and the inflammatory cytokines: interleukin-1 alpha (IL-1α), interleukin 6 (IL-6), interleukin 8 (IL-8), monocyte chemoattractant protein-1 (MCP-1), and macrophage inflammatory protein-1 alpha (Mip-1 alpha) were quantitated, showing notable detectable protein levels in the culture media of all groups. Among these, BDNF, known to promote RGC survival, was significantly more highly expressed than the other growth factors in all groups. Additionally, there was no significant difference in the levels of the immune response-associated cytokines between the control and PBG-based scaffold groups, suggesting that the peptide polymers do not elicit an immune response in hiPSC-derived RGCs in vitro Fig. 4 (b). Next, the in vivo biocompatibility of the three types of PBG-based scaffolds was investigated by implanting them into the vitreous body of mice. The inflammatory response and immune cell infiltration in the retina were then examined using hematoxylin and eosin staining of the tissue. No obvious inflammatory response was observed, and there was no difference in staining between the retina of control mice and that of mice implanted with the scaffolds for 2 weeks, indicating that all three scaffolds were biocompatible Fig. 4 (c).

3.5. hiPSC-derived RGCs show the best electrophysiological activity when cultured on the PBGA20-Na scaffold

Since PBGA20-Na, which contains sodium salt, demonstrated better ionic conductivity compared to the PBGA20 scaffold Fig. S2 (a and b), the question arises whether these favorable electrochemical properties can contribute to the electrophysiological activity of hiPSC-derived RGCs cultured on the PBG-based scaffolds. The electrophysiological activity of hiPSC-derived RGCs was recorded to determine whether there was a difference in electrophysiology between hiPSC-derived RGCs cultured on the PBG-based scaffolds and those grown on the cover glass. Because the spiking responses elicited by hiPSC-derived RGCs cultured on the PBGA20 and PBGA20-Na groups were only captured after 60 days, we analyzed the electrophysiological activity of hiPSC-derived RGCs in all groups after 60 and 100 days of adherent culture. As shown by the patch-clamp recordings Fig. 5 (a), hiPSC-derived RGCs cultured on the PBGA20 and PBGA20-Na scaffolds already had a clear response to the current injection on D60, and they were able to fire action potentials when a current of 70 nA was applied Fig. 5 (b). On D100, more robust action potentials could be evoked in hiPSC-derived RGCs cultured on the PBG-based scaffolds, even with a lower current series of 50 nA. Statistical analysis of the numbers of hiPSC-derived RGCs that fired action potentials in the PBG-based scaffold groups and revealed that hiPSC-derived RGCs cultured on the PBGA20 and PBGA20-Na scaffolds demonstrated much stronger electrophysiological activities than those cultured on the cover glass at D60 and D100 Fig. 5 (c). Moreover, hiPSC-derived RGCs cultured on PBGA20 and PBGA20-Na scaffolds showed significantly higher AP peaks compared to those cultured on the cover glass during the applied currents of 70 nA and 50 nA, on D60 and D100, respectively. On D100, the highest AP peaks were observed in hiPSC-derived RGCs cultured on PBGA20-Na scaffolds Fig. 5 (d). Additionally, rapid inward currents of excitatory postsynaptic currents (EPSCs) were observed in hiPSC-derived RGCs on the PBGA20 and PBGA20-Na scaffolds on D60 and were also recorded in hiPSC-derived RGCs on all three PBG-based scaffolds on D100. By contrast, neither the firing of action potentials nor EPSCs were observed in hiPSC-derived RGCs cultured on the cover glass on D60 and D100 Fig. 5 (e and f). These data suggest an earlier occurrence of spiking responses in hiPSC-derived RGCs cultured on PBGA20 and PBGA20-Na scaffolds. Furthermore, hiPSC-derived RGCs demonstrated better electrophysiological activity with higher AP peaks while cultured on the PBGA20-Na scaffold.

4. Discussion

Appropriate 3D scaffolds with specific structural and biochemical features, such as our PBG-based scaffolds, have gained attention due to their ability to enhance efficiency and manipulate neurite outgrowth [17–19]. Our present study aims to address this issue by demonstrating the ability to generate a substantial number of human-induced pluripotent stem cell (hiPSC)-derived RGC progenitors using a PBG-based biocompatible scaffold. This study provides a comprehensive evaluation of the impact of the PBG-based scaffolds on the morphological, molecular, and electrophysiological characteristics of hiPSC-derived RGCs. We have successfully integrated the physical, biochemical, and electroactive properties beneficial to neuronal growth into the PBG-based scaffolds. Among them, PBGA20-Na peptide-based scaffold has been found to best enhance structural and functional maturation of hiPSC-derived RGCs, in terms of neuronal differentiation, neurite outgrowth, and electrophysiological activity.

Previous studies showed that carbon nanotube PLGA-based scaffolds [20] offer adjustable physical properties that make them advantageous for RGC growth. However, the biocompatibility of carbon nanotubes in complex environments such as the human body might raise concerns when considering application. S. Behtaj et al. developed and employed a different scaffold, PGS/PCL (poly(glycerol sebacate)/polycaprolactone) electrospun scaffold, to culture RGCs derived from human embryonic stem cells [17], and demonstrated enhanced differentiation of hESCs into RGC-like cells and directed growth of RGC neurites. However, their results indicated that the neurite lengths of cells cultured on their control group (TCP group) were comparable to or longer than those in the PGS/PCL group. Our findings of this study revealed that the neurites of hiPSC-derived RGC progenitors exhibited extended growth along the fibers of the PBG-based scaffolds without obvious cytotoxicity for retina tissue, indicating that the scaffolds could support cell adherence and facilitate growth. Our previous work had shown that PBG scaffold was beneficial to the neurite growth of hiPSC-derived RGC in all directions [16]. However, according to our present data shown in Fig 2d, the neurites were highly oriented along the PBG-based fibers, proving that the alignment of fibers plays a significant role in guiding their directional growth. This observation suggests the potential of PBG-based scaffolds, especially PBGA20-Na, in promoting directed neurite outgrowth and axon formation in hiPSC-derived RGCs, thereby improving their clinical relevance.

In order to validate the acquisition of differentiated RGCs, multiple RGC markers are commonly utilized. For example, Kobayashi et al. characterized iPSC-derived RGCs using biomarkers such as ATOH7, BRN3B, and ISL1 [21]. In this study, we also used immunostaining analysis of neuronal (TUJ1) and RGC protein markers (BRN3B, MATH5, and ISLET1) to reveal that the expression levels of these markers in hiPSC-derived RGCs increased significantly over time. Statistical analysis indicated a significant difference in MATH5 expression between the PBGA20-Na group and the control group on Day 7. Conversely, the expression levels of retinal progenitor cell markers (Rx, Pax6, and Chx10) decreased as time progressed. These findings suggest that the differentiation of hiPSCs toward the RGC lineage is enhanced with scaffolds, particularly with higher efficiency when using the PBGA20-Na scaffold.

Previous studies have indicated the involvement of the glutamate signaling pathway in neuronal development, including dendritic development and regulation [22,23], through initiation of the opening of calcium channels and subsequent activation of various downstream signaling pathways [24,25]. However, excessive glutamate

concentration can lead to degeneration of retinal ganglion cells (RGCs) [26]. In our study, we measured the concentration of glutamate in culture media with and without cells. Our findings suggest that all three PBG-based scaffolds with cells exhibited higher glutamate concentrations compared to the control group, with the PGBA20-Na group showing the highest concentration. This implies that the PBG-based scaffolds may facilitate the neuronal release of glutamate or that the relatively more mature state of RGCs in the PBGA20-Na group contributed to this result. The media-only group also demonstrated some difference among the four groups but without statistical significance, which may infer that a trace amount of glutamate could be resolved from the scaffold.

Our previous studies have already confirmed that PBG-related scaffolds, with or without electrical stimuli, can promote directional neurite outgrowth in PC-12 neuronal cells [15]. The results provided us proof of concept but not enough for translational applications. Therefore, in this study, we further explored and found that, among these scaffolds, PBGA20-Na, which possesses the highest electrical conductance, yielded the most favorable outcomes with the hiPSC-derived RGCs model and from an electrophysiological point of view, which could be a valuable resource for future cell replacement therapies. Functionally, we observed that both the PBGA20 and PBGA20-Na groups exhibited earlier and more pronounced electrophysiological activity compared to the other groups. The exposed COO− groups of PBGA20 and PBGA20-Na may attract electrolytes in the solution, facilitating charge transfer and lowering the threshold for action potential initiation. According to our data shown in Fig S2, the ionic conductivity was even better in the PBGA20-Na group than the PBGA20 group, and Fig 2c also showed that the average neurite length was statistically longer in the PBGA20-Na group than the PBGA20 group in both D3 and D7. Therefore, we truly believed that electrical properties played an important role in neurite outgrowth. Additionally, the increased concentration of free glutamate and the potential effects of glutamate subunits on the polymers may contribute to the earlier electrophysiological maturation of iPSC-induced RGCs. In conclusion, the electroactive properties of the PBGA20 and PBGA20-Na scaffolds may enhance the functional development and activity of iPSC-induced RGCs, which could be a resource of cell therapy for optic nerve regeneration.

In summary, we have successfully combined physical, biochemical, and electroactive advantages into the PBG-based scaffolds. This study demonstrated that PBG-based scaffolds, especially PBGA20-Na, exert positive effects on the morphological, molecular, and electrophysiological development of hiPSC-derived RGCs. Looking forward to the future, further efforts would need to explore the long-term performance of cell-substrate interactions, particularly in an *in vivo* large-animal model setting and, given the excellent results of directional neurite outgrowth on the scaffolds, we may try to explore the extent of topographic arrangement achievable with the PBGA20-Na scaffold on the inner retina surface.

In conclusion, the collective findings of our study underscore the importance of offering appropriate structural support to guide the directional outgrowth of neurites from hiPSC-derived RGCs. The incorporation of glutamic acid and the promotion of cellular electrophysiological activity facilitated by PBG-based scaffolds, particularly the PBGA20-Na scaffold, play crucial roles in enhancing the growth and maturation of hiPSC-derived RGCs. These promising results provide a foundation for potential sheet transplantation of RGCs as a cell therapy for optic neuropathy.

Ethics approval and consent to participate

All mouse experiments were approved by the Institutional Animal Care and Use Committee of the Laboratory Animal Center, National Taiwan University College of Medicine (IACUC approval number: 20190102). Data of approval: January 2nd, 2019.

Consent for publication

Not applicable.

Availability of data and materials

All data are available from the corresponding authors upon reasonable request.

Funding

This work was supported by the Ministry of Science and Technology, Taiwan [grant numbers: MOST-106-2314-B-002-128-MY2, MOST-108-2314-B-002-065-MY, and MOST108-2221-E-002-027-MY3].

CRediT authorship contribution statement

Ta-Ching Chen: Conceptualization, Methodology, Validation, Formal analysis, Writing – review & editing. **Yu-Ju Minnie Chou:** Validation, Investigation. **Yu-Xuan Wu:** Writing – review & editing. **Jui-En Lo:** Writing – review & editing. **Chia-Yu Lin:** Writing – review & editing. **Yun-Hsiu Tseng:** Writing – review & editing. **Ya-Chun Chu:** Writing – review & editing. **Wei-Li Chen:** Writing – review & editing. **Fung-Rong Hu:** Writing – review & editing. **Wei-Fang Su:** Methodology, Validation, Formal analysis, Writing – review & editing. **Hung-Chih Kuo:** Methodology, Validation, Writing – review & editing.

Declaration of Competing Interest

The authors have no competing interests related to this study to declare.

Acknowledgements

We thank the staff of the Seventh Core Laboratory, Department of Medical Research, National Taiwan University Hospital for their technical support during the study.

Supplementary materials

Supplementary material associated with this article can be found, in the online version, at doi:10.1016/j.jtice.2023.105257.

References

[1] Newman NJ. Optic neuropathy. Neurology 1996;46(2):315–22.
[2] Bourne RR, Taylor HR, Flaxman SR, Keeffe J, Leasher J, Naidoo K, et al. Number of people blind or visually impaired by glaucoma worldwide and in world regions 1990–2010: a meta-analysis. PLoS One 2016;11(10):e0162229.
[3] Quigley HA, Broman AT. The number of people with glaucoma worldwide in 2010 and 2020. Brit J Ophthalmol 2006;90(3):262–7.
[4] Tham YC, Li X, Wong TY, Quigley HA, Aung T, Cheng CY. Global prevalence of glaucoma and projections of glaucoma burden through 2040: a systematic review and meta-analysis. Ophthalmology 2014;121(11):2081–90.
[5] Khatib T, Martin K. Protecting retinal ganglion cells. Eye 2017;31(2):218–24.
[6] Dahlmann-Noor A, Vijay S, Limb GA, Khaw P. Strategies for optic nerve rescue and regeneration in glaucoma and other optic neuropathies. Drug Discov Today 2010;15(7-8):287–99.
[7] Zhang J, Wu S, Jin ZB, Wang N. Stem cell-based regeneration and restoration for retinal ganglion cell: Recent advancements and current challenges. Biomolecules 2021;11(7):987.
[8] Mead B, Berry M, Logan A, Scott RA, Leadbeater W, Scheven BA. Stem cell treatment of degenerative eye disease. Stem Cell Res 2015;14(3):243–57.
[9] Seyedrazizadeh SZ, Poosti S, Nazari A, Alikhani M, Shekari F, Pakdel F, et al. Extracellular vesicles derived from human ES-MSCs protect retinal ganglion cells and preserve retinal function in a rodent model of optic nerve injury. Stem cell Res Ther 2020;11(1):1–13.
[10] Baraniak PR, McDevitt TC. Stem cell paracrine actions and tissue regeneration. Regen Med 2010;5(1):121–43.
[11] Kuo YC, Hong MY, Rajesh R. Regeneration of insulin-producing cells from iPS cells using functionalized scaffolds and solid lipid nanoparticles. J Taiwan Inst Chem Eng 2022;135:104387.

[12] Kuo YC, Tsao CW, Rajesh R. Dual-sized inverted colloidal crystal scaffolds grafted with GDF-8 and Wnt3a for enhancing differentiation of iPS cells toward islet β-cells. J Taiwan InstChem Eng 2021;126:371–82.
[13] Kuo YC, Lee IH, Rajesh R. Self-assembled ternary poly (vinyl alcohol)-alginate-gelatin hydrogel with controlled-release nanoparticles for pancreatic differentiation of iPS cells. J Taiwan InstChem Eng 2019;104:27–39.
[14] Kuo YC, Hsu CC, Rajesh R. iPSCs-laden GDF8-grafted aldehyde hyaluronic acid-polyacrylamide inverted colloidal crystal constructs with controlled release of CHIR99021 and retinoic acid to generate insulin-producing cells. J Taiwan InstChem Eng 2020;116:223–37.
[15] Lin CY, Luo SC, Yu JS, Chen TC, Su WF. Peptide-based polyelectrolyte promotes directional and long neurite outgrowth. ACS Appl Bio Mater 2018;2(1):518–26.
[16] Chen TC, She PY, Chen DF, Lu JH, Yang CH, Huang DS, et al. Polybenzyl glutamate biocompatible scaffold promotes the efficiency of retinal differentiation toward retinal ganglion cell lineage from human-induced pluripotent stem cells. Int J Mole Sci 2019;20(1):178.
[17] Behtaj S, Karamali F, Najafian S, Masaeli E, Esfahani MHN, Rybachuk M. The role of PGS/PCL scaffolds in promoting differentiation of human embryonic stem cells into retinal ganglion cells. Acta Biomater 2021;126:238–48.
[18] Luo Z, Xian B, Li K, Li K, Yang R, Chen M, et al. Biodegradable scaffolds facilitate epiretinal transplantation of hiPSC-Derived retinal neurons in nonhuman primates. Acta Biomater 2021;134:289–301.
[19] Kador KE, Alsehli HS, Zindell AN, Lau LW, Andreopoulos FM, Watson BD, et al. Retinal ganglion cell polarization using immobilized guidance cues on a tissue-engineered scaffold. Acta Biomater 2014;10(12):4939–46.
[20] Yang R, Yang S, Li K, Luo Z, Xian B, Tang J, et al. Carbon nanotube polymer scaffolds as a conductive alternative for the construction of retinal sheet tissue. ACS Chem Neurosci 2021;12(17):3167–75.
[21] Kobayashi W, Onishi A, Tu HY, Takihara Y, Matsumura M, Tsujimoto K, et al. Culture systems of dissociated mouse and human pluripotent stem cell–derived retinal ganglion cells purified by two-step immunopanning. Investig Ophthalmol Vis Sci 2018;59(2):776–87.
[22] Elias E, Yang N, Wang P, Tian N. Glutamate activity regulates and dendritic development of J-RGCs. Front Cell Neurosci 2018;12:249.
[23] Deplano S, Gargini C, Maccarone R, Chalupa LM, Bisti S. Long-term treatment of the developing retina with the metabotropic glutamate agonist APB induces long-term changes in the stratification of retinal ganglion cell dendrites. Develop Neurosci 2005;26(5-6):396–405.
[24] Augustine GJ, Santamaria F, Tanaka K. Local calcium signaling in neurons. Neuron 2003;40(2):331–46.
[25] Hartwick AT, Hamilton CM, Baldridge WH. Glutamatergic calcium dynamics and deregulation of rat retinal ganglion cells. J Physiol 2008;586(14):3425–46.
[26] Boccuni I, Fairless R. Retinal glutamate neurotransmission: from physiology to pathophysiological mechanisms of retinal ganglion cell degeneration. Life 2022;12(5):638.